Song, L.; Hu, X.; Wang, L.; Stark, A.; Lazurenko, D.; Lorenz, U.; Lin, J.; Pyczak, F.; Zhang, T.:

Microstructure evolution and enhanced creep property of a high Nb containing TiAl alloy with carbon addition.

In: Journal of Alloys and Compounds. Vol. 807 (2019) 151649.
First published online by Elsevier: 31.07.2019

https://dx.doi.org/10.1016/j.jallcom.2019.151649

Microstructure evolution and enhanced creep property of a high Nb containing TiAl alloy with carbon addition

Lin Song[1,2]*, Xinguo Hu[1], Li Wang[2]*, Andreas Stark[2], Daria Lazurenko[3], Uwe Lorenz[2], Junpin Lin[4], Florian Pyczak[2], Tiebang Zhang[1]

[1]State Key Laboratory of Solidification Processing, Northwestern Polytechnical University, Xi'an, Shaanxi 710072, China
[2]Institute of Materials Research, Helmholtz-Zentrum Geesthacht, Max Planck-Str. 1, Geesthacht, D-21502, Germany
[3]Novosibirsk State Technical University, Karl Marks str. 20, Novosibirsk, 630073, Russia
[4]State Key Laboratory for Advanced Metals and Materials, University of Science and Technology Beijing, Beijing 100083, China
Corresponding authors: Lin Song (songlin@nwpu.edu.cn, lin.song@hzg.de), Li Wang (li.wang1@hzg.de)

Abstract

The microstructure evolution and carbide precipitation in a Ti-46Al-8Nb-0.7C alloy as well as its creep properties at intermediate temperatures are investigated by high-energy X-ray diffraction and electron microscopy. The alloy with a nearly fully lamellar microstructure exhibits excellent creep resistance, which could be attributed to the good microstructural stability and strengthening effects from both P- and H-carbides. It is also found that the creep parameters have different effects on the precipitation of the carbides. The overall volume fraction of the carbides shows a positive correlation with the creep temperature and time. However, the thermal stability of P-carbides in the γ grain interior decreases at a higher creep temperature. The creep stress hardly affects the precipitation and morphology development of the P-carbides. On the contrary, a higher stress can promote the H-carbide formation at the γ/α_2 interfaces via α_2 lath decomposition in lamellar colonies.

Keywords

TiAl alloys; precipitation; phase transitions; creep properties; transmission electron microscopy, TEM; synchrotron radiation.

1. Introduction

As a new class of intermetallic structural materials, high Nb-containing TiAl alloys (high Nb-TiAl alloys) have achieved significant development in the recent years and

show promising applications in the aerospace and automotive markets [1-4]. Systematical studies have been conducted to understand and improve the creep behavior of high Nb-TiAl alloys [5-9]. Numerous studies revealed that the fully lamellar microstructure with high amounts of anisotropic laths showed better creep resistance than the nearly lamellar and duplex microstructures [4, 10]. Meanwhile, the microstructural stability is important for the creep life of high Nb-TiAl alloys. For blade application, γ-TiAl alloys are expected to have a good microstructure stability to achieve a long creep life with a small creep strain [3]. The microstructural degradation via the decomposition of α_2 laths and the discontinuous precipitation at lamellar boundaries during the creep process deteriorates the creep resistance significantly [10-12]. Thus, a better creep strength can be achieved by appropriate alloying and annealing treatment to stabilize the microstructure. Zhu et al. reported that after annealing a Ti-47Al-2Nb-2Mn (all compositions are given in at.% unless indicated otherwise) + 0.8 vol.% TiB_2 alloy at 1000 °C for 8 h the microstructure was destabilized due to the volume fraction decrease of the α_2 phase, resulting in a better creep resistance than the microstructure without annealing treatment [10]. The creep resistance of a Ti-43.5Al-4Nb-1Mo-0.1B-0.3C-0.3Si alloy was enhanced by decreasing the lamellar interface spacing as the lamellae interfaces impeded the motion of ordinary dislocations [8]. However, Zhu et al. reported that the lamellar refinement was important for improving the creep resistance at primary creep stage in a Ti-45Al-2Nb-2Mn+0.8 vol.%TiB_2 alloy, but detrimental for the total creep life since the fine lamellar microstructure was susceptible to deformation-induced spheroidization [13]. Besides, the equiaxed grains at lamellar boundaries which were resulted from spheroidization provoked easy dislocation motion and deteriorated the creep resistance [11]. Thus, the further enhancement of creep resistance can be obtained by microstructural optimization. It is reported that carbon addition can improve the creep properties of TiAl alloys via solid-solution and precipitation strengthening depending on the carbon content [14-17]. Klein et al. claimed that the addition of carbon stabilized the α_2 phase and hindered the precipitation of γ and β_o (ω_o) phases [18]. Park et al. reported that the addition of carbon increased the heterogeneous nucleation rate of the γ laths effectively, resulting in a reduction of the lamellar spacing within the lamellar colonies and thus improving the creep resistance [19]. During the annealing and creep processes, the perovskite (P-) type carbides and hexagonal (H-) type carbides precipitate in the γ phase, at the lamellar interfaces and grain boundaries. It is believed that the carbides are effective pinning obstacles for dislocations in carbon containing TiAl alloys [15, 17, 20]. Schwaighofer et al. found that some P-carbides nucleated at dislocations, which were deformation-induced during creep [15]. Christoph et al. revealed that a fine dispersions of P-carbides formed arrays of strong glide obstacles for perfect and twinning partial dislocations after compression at room temperature [17]. Wang et al. reported that the P-carbides

undergone continuous morphology development when annealed at a temperature range from 800 to 1000 °C [21-23]. It is found that the P-carbides grew, coarsened and split eventually during annealing [22, 23]. H-carbides usually form at grain boundaries and in the γ grains with coarse particle size with the relationship $[101]\gamma//[11\bar{2}0]H$; $(11\bar{1})\gamma//(0001)H$ [23]. Lapin et al. claimed that the formation of primary H-carbides could improve the creep resistance of Ti-46.4Al-5.1Nb-1C-0.2B alloy during creep from 800 to 950 °C [24]. However, the morphology development of carbides during creep still needs further investigation. Besides, the effects of creep parameters on the formation of P-carbides and H-carbides are still not clear.

In the present work, the strengthening mechanisms and microstructure evolution in the C-containing high Nb-TiAl alloys during creep are characterized. The effects of the creep temperature and stress on the stability of the lamellar structure and formation of P- and H-carbides are also discussed. The results of this study could be instructive for further improving the creep properties of TiAl alloys with addition of carbon.

2. Experimental details

The alloy with a nominal composition of Ti-46Al-8Nb-0.7C was prepared in a non-consumable arc melting furnace in an argon atmosphere. A cylindrical ingot measured about Φ130 mm×300 mm was re-melted 4 times to ensure compositional homogeneity. Then the ingot was hot isostatic pressing (HIPed) at 1270 °C under a pressure of 130 MPa for 4 h and then cooled in furnace. Cylinder samples with a size of 10 mm in diameter and a gauge section of Φ5.3×27.3 mm were cut for creep tests from the center of the upper part of the as-HIPed ingot. The creep tests were performed under a constant load in a SATEC M3 creep machine at 750 and 850 °C under tensile loading of 130 and 260 MPa in air. To study the microstructural evolution during creep, four creep tests were interrupted before specimen failure. Two tests were stopped at a creep time of 1200 h at 750 °C under 130 and 260 MPa and the other two were interrupted at a creep time of 110 h under 850 °C/260 MPa and 1100 h under 850 °C/130 MPa. All the specimens after the creep test were cut into two parts, namely the gauge and holder section. The gauge section was the loaded part with stress and thermal exposure applied while the holder section was the specimen head used to mount it in the creep machine, which only underwent thermal exposure at the creep temperature. The microstructures before and after the creep tests were investigated on a Zeiss GEMINI 1530 field emission scanning electron microscope (SEM) using the back-scattered electron (BSE) mode and on a FEI Titan 80-300 field emission transmission electron microscope (TEM) operated at 300 kV. The SEM and TEM samples were cut along and perpendicular to the loading direction, respectively. Thin TEM foils were mechanically ground to 0.1 mm and then prepared by twin-jet electro-polishing in a solution of 30 ml perchloric acid, 175 ml butanol, and 300 ml methanol at 30 V and -30 °C. Room-temperature high-

energy X-ray diffraction (HEXRD) measurements were conducted at the HEMS beam line run by the Helmholtz-Zentrum Geesthacht at the Deutsches Elektronen-Synchrotron (DESY) in Hamburg. The beam size was 0.5 mm × 0.5 mm and the wavelength 0.14235 Å. The reflections were recorded with a PerkinElmer XRD 1621 flat panel detector. The weight fractions of the majority phases (γ and α_2) was analyzed by the Rietveld method, while the fractions of the P- and H-carbides could not be determined using this method due to their small contents.

3. Results and discussion

3.1 As-HIPed microstructure

Fig. 1 shows the microstructure and phase constitution of the as-HIPed sample before creep test. A nearly fully lamellar microstructure composed of large lamellar colonies and a small amount of equiaxed γ grains is shown in Fig. 1a. The average size of the lamellar colonies is about 200 μm. The β_o and ω_o phases, which are frequently found in high Nb-containing TiAl alloys, are not observed [25, 26]. As marked by the arrows in Fig. 1b, some fractured α_2 laths are observed at the lamellar colonies, which formed during the furnace cooling process after HIP via the "parallel decomposition" mechanism [27, 28]. In addition, some needle- or plate-like dark features marked in Fig. 1a can be observed, which might be due to the falling out of the large H-carbides during specimen preparation. According to the HEXRD spectrum shown in Fig. 1c, the diffraction peak of {106} planes of the H-carbides is clearly detected, while no reflections from the P-carbides show up. On the contrary, in our previous studies in the HIPed Ti-45Al-5Nb-0.75C alloy with a similar carbon concentration, H-carbides were only occasionally observed while P-carbides were commonly detected at grain boundaries [29, 30]. By analyzing the HEXRD spectrum, the weight fraction of the α_2 phase was determined to be 12.9 wt.% in the present as-HIPed alloy and is lower than 18 wt.% determined in the Ti-45Al-5Nb-0.75C alloy. This could explain a higher volume fraction of the H-carbides found in the Ti-46Al-8Nb-0.7C alloy as a decrease in the α_2 phase amount can promote the carbide formation [21]. In order to know whether P-carbides have formed in the HIPed Ti-46Al-8Nb-0.7C alloy, the specimen was further investigated by TEM.

The TEM images in Fig. 2 confirm the existence of the P-carbides in the HIPed Ti-46Al-8Nb-0.7C alloy. P-carbides have formed at grain boundaries and interfaces, at dislocations (Fig. 2a) and in the γ laths as well as the equiaxed γ grains (Fig. 2b). All the P-carbides exhibit the orientation relationship $[001]_\gamma//[001]_P$ and $(100)_\gamma//(100)_P$ with the γ matrix. The precipitates in the γ grains have a well-reported needle-like morphology with the long axis parallel to the $[001]_\gamma$ zone axis [23]. Thus, they show dot-like cross-sections when viewed along the $[001]_\gamma$ direction as shown in Figs. 2b and

c. Additionally, “coffee-bean” contrast is visible around the carbides in Fig. 2b due to the strain field caused by the coherent stress. As evidenced in Fig. 2c, the interface between the γ matrix and the P-carbide is coherent. According to the HEXRD investigation, the lattice parameters of the γ matrix and P-carbides are a_γ=0.402 nm, c_γ=0.408 nm, and a_p=0.415 nm, respectively. The lattice misfit between the P-carbides and the γ matrix along the $[001]_\gamma$ and $[100]_\gamma$ directions can be calculated by the following equations: $\varepsilon_{100}=(a_P-a_\gamma)/a_P$ and $\varepsilon_{001}=(a_P-c_\gamma)/a_P$, indicating a smaller lattice misfit of 1.7 % along the $[001]_\gamma$ orientation compared to 3.1 % along the $[100]_\gamma$ direction. Therefore, the P-carbides in the γ matrix prefer to grow along the $[001]_\gamma$ direction, forming a needle-like shape to reduce the misfit in the $[100]_\gamma$ and $[010]_\gamma$ directions, which is in accordance with that reported in [23]. Previous studies proved that P-carbides could be dissolved at temperatures above 1100 °C, indicating that the observed P-carbides in the HIPed sample precipitated during the furnace cooling [29].

3.2 Creep test results

The creep test results are shown in Fig. 3 and Table. 1. The creep time until failure is 850 h for the sample tested at 850 °C/260 MPa and 3267 h for the sample tested at 850 °C/130 MPa. The creep curve of the sample crept at 850 °C/130 MPa exhibits a short primary creep stage and a long secondary creep stage. When the creep time reaches 3200 h, a short accelerated tertiary creep stage is observed. The sample crept at 750 °C/260 MPa has reached 8500 h without rupture. Table 2 summarizes the creep properties of the high Nb-TiAl alloys reported in literature. It is found that the high Nb-TiAl alloys with duplex microstructures show significantly lower creep resistance and the alloys are easier to deform during creep [31]. The carbon containing TiAl alloys have a longer creep life but smaller creep fracture strain than the carbon-free alloys with similar compositions [5-7]. Compared with the results in Table 2, the Ti-46Al-8Nb-0.7C alloy exhibits better creep resistance with a longer creep life but a limited creep strain, which is, despite the creep strain, apparently superior to the reported alloys with varied compositions.

In the following, the microstructure evolution during creep tests will be examined by SEM, HEXRD and TEM in order to understand the influences of test conditions on the microstructure and thus creep properties of the Ti-46Al-8Nb-0.7C alloy.

3.3 Influences of stress and temperature on microstructure evolution

3.3.1 SEM observation

Fig. 4 shows the microstructure of the samples crept at 850 ℃. At this temperature, with increasing creep time, more and more carbides (both P- and H-types) form at different positions. Due to the large sizes, some coarsened P-carbides at grain

boundaries can also be identified in the SEM images (for example at grain boundaries in Fig. 4f). After creep under 260 MPa for 110 h, in the gauge section (Fig. 4a) the α_2 laths in some lamellar colonies start to decompose via the "parallel decomposition" [28], resulting in the coarsening of neighboring γ laths. Besides, numerous needle- or plate-like precipitates with varied sizes are observed along the decomposed α_2 laths, which are H-carbides that form at the expense of the α_2 phase [21, 32-34]. In contrast, in the holder section (Fig. 4b), the α_2 laths do not change obviously, i.e. nearly no decomposition of the α_2 phase occurs. With extending creep time to 850 h and above, the α_2 lath decomposition in some lamellar colonies is more significant in the gauge section (Fig. 4c). Additionally, some lamellae are curved near grain boundaries and cavities form along the lamellar boundaries due to grain boundary sliding effects (Fig. 4d), which can initiate crack propagation along colony boundaries [9, 35, 36]. In the holder section, α_2 laths in some lamellar colonies also decompose and H-carbides form and consume the α_2 phase (Fig. 4e). However, no curved lamellae or cavities are observed (Fig. 4f). The difference in microstructure evolution between the gauge and holder sections should be due to the different stress conditions in the two sections. At a short creep time (110 h), in the gauge section the α_2 laths tend to decompose due to the applied stress while in the holder section where the stress should be nearly absent, the α_2 laths are relatively thermally stable. With continuing creep to 850 h, the α_2 laths in the holder section also start to decompose, as they are not thermodynamically stable at this temperature.

The thermal stability of the α_2 laths is higher under a smaller stress of 130 MPa. After creep for 1100 h, the α_2 laths in the lamellar colonies only show a slight decomposition (Fig. 4g). After further creep until fracture for the extended period of 3267 h, the α_2 laths in the lamellar colonies decompose significantly with formation of numerous H-carbides at the expense of the α_2 phase (Fig. 4h). In addition, the lamellae are severely deformed (curved and broken) and numbers of fine equiaxed γ grains in sizes of less than 10 μm form at the lamellar boundaries. Previous studies hint that the equiaxed γ grains with fine grain size could deteriorate the creep resistance [11-13]. Compared to the limited width of the γ laths, dislocation gliding in the equiaxed γ grains can be easier since there is more free space in various directions. However, the glide distance of dislocations in these γ grains is still limited because of the small grain sizes. As a result, stress can be accumulated at the grain boundaries. Together with the carbide precipitation at the boundary, the initiation of cracks is prone to happen in the positions where coarse carbides appear. Moreover, the increased grain boundary surface also facilitates grain boundary gliding, leading to the formation of cavities. In fact, the cracks along the lamellar colony boundaries are commonly observed in the failed creep samples.

The lamellar microstructures in the gauge section of the samples crept at 750 ℃ under

130 and 260 MPa for 1200 h are shown in Fig. 5. It is found that the α_2 laths are also stable at a lower temperature. Again, with increasing stress, α_2 laths decompose more significantly and more H-carbides form at the primary α_2 lath position. Thus, from the above results, it can be concluded that the creep temperature and stress can strongly influence the stability of the lamellar structure. A higher creep temperature and stress can promote the α_2 lath decomposition, resulting in the formation of the H-carbides at their locations at the expense of α_2 phase.

3.3.2 HEXRD investigations

Fig. 6 shows the HEXRD spectrums for the creep specimens tested at different conditions. The microstructure is mainly composed of the γ phase with a weight fraction of around 90-95%. The fraction of α_2 phase is reduced compared to that in the HIPed state and the detailed values in the holder section at different creep conditions are listed in Table 3. The results show that the α_2 phase fraction decreases with increasing creep temperature and time due to continuous $\alpha_2 \rightarrow \gamma$+H-carbide phase transformation during the creep process. This phenomenon has also been found in a former study in the Ti-45Al-5Nb-0.5/0.75C alloys after annealing at different temperatures and times [21]. From Figs. 4 and 5 it is clearly shown that an increase in creep stress promotes the decomposition of the α_2 laths in the gauge section. Thus, by increasing creep temperature, stress and time, the α_2 laths decompose more significantly, resulting in the γ lath coarsening and the formation of H-carbides at the expense of the α_2 phase.

The fractions of the P- and H-carbides could not be determined using the Rietveld analysis that was applied to calculate the α_2 phase fraction due to their small contents. A rough estimation on the carbide fraction evolution when altering the creep time, stress and temperature can be made based on the change on the intensity of the carbide reflections. For this, it is assumed that the γ phase is the majority phase and its fraction remains the same when test parameters change. In Fig. 6, all the HEXRD spectrums were normalized to the highest reflection $\{111\}_\gamma$. For the specimen crept 850 °C and 260 MPa for 110 h, the P-carbide fraction shows no clear difference in the holder and gauge sections as the intensity of the $\{111\}_P$ and $\{200\}_P$ peaks in these two sections is similar. While, the fraction of the H-carbides is obviously higher in the gauge section than in the holder section due to a high intensity of the $\{106\}_H$ peak in the gauge section. This agrees with the SEM observation in Figs. 4a and b that the α_2 laths decompose and H-carbides form in the gauge section. After creep at 850 °C and 130 MPa for 1100 h, the fractions of the P- and H-carbides did not vary a lot in the holder and gauge sections indicated by the similar intensity of the carbide reflections. This hints that the stress condition difference between the holder and gauge sections did not influence the precipitation of the P- and H-carbides after a very long creep time. In addition, it is found that the volume fractions of the P- and H-carbides in the specimen after creep at

850 °C and 130 MPa for 1100 h are much higher than those in the specimen after creep at 850 °C and 260 MPa for 110 h as can be concluded from the higher carbide peak intensity in the former alloy. This seems to contradict the SEM observation that more α_2 laths are found to decompose and more H-carbides form in the lamellar colonies in the specimen crept for 110 h. However, it should be kept in mind that carbides also form in the γ matrix, at interfaces and grain boundaries that account for the majority of the carbide fraction. Thus, it can be concluded that the carbides form and grow continuously with increasing creep time and the carbide precipitation might not reach the thermodynamically equilibrium condition even after creep for 1100 h. At a lower creep temperature of 750 °C, the P-carbide fraction also does not vary a lot in the holder and gauge sections when the creep stress is changed as a similar intensity is found for the $\{111\}_P$ or $\{200\}_P$ peak. While, the fraction of the H-carbides is always higher in the gauge sections of the specimens under a higher creep stress due to the larger amount of α_2 lath decomposition as shown in Fig. 5. Compared with the situation after creep at 850 °C, the influence of the stress on the formation of H-carbides is found after creep for 1200 h at 750 °C. It could be inferred that this influence will be eliminated after a longer creep time when the precipitation of the carbides gets close to the thermodynamic equilibrium condition. With respect to the influence of the creep temperature on carbide formation, the spectrums tested at the same creep stress and for a similar time, i.e. at 850 °C, 130 MPa, 1100 h and at 750 °C, 130 MPa, 1200 h, are compared. It is found that both the P- and H-carbide fractions increase with creep temperature as the $\{111\}_P$, $\{200\}_P$ and $\{106\}_H$ peak intensities are higher at 850 °C. Thus, a higher creep temperature promotes the formation of both P- and H-carbides due to a smaller α_2 phase fraction at a higher temperature.

3.3.3 TEM observation of carbide formation during creep

As shown in the above results, P-carbides have already formed at dislocations, at interfaces and grain boundaries, and in the γ phase in the HIPed state. With further annealing during creep, more P-carbides would form at these locations. Compared to the coarse H-carbides, P-carbides commonly have smaller sizes. Fig. 7 shows the P-carbide precipitation in specimens crept at 750 °C for 1200 h. As already known from the HEXRD results, the creep stress has no obvious influence on the P-carbide fraction. Also in the TEM observation, the distribution and morphology evolution of the P-carbides was found to be similar for different creep stresses. As shown in Figs. 7a-c, after creep at 750 °C for 1200 h, numerous P-carbides are present at dislocations, at lamellar interfaces, in the γ laths and in equiaxed γ grains. However, the deformation seems not severe in the γ phase after creep for 1200 h as only few dislocations are found. With further creep deformation, it is expected that the P-carbides can efficiently hinder the dislocation glide in the γ phase and thus contribute to a long creep life of the alloy.

Additionally, the morphology of P-carbides in the γ phase has changed from needles into conglomerates of small sub-particles by splitting. The conglomerates of sub-particles resemble a plate-like morphology with the plate planes parallel to the $(100)_\gamma$ and $(010)_\gamma$ crystallographic planes. So when viewed along the $<100]_\gamma$ orientation, two sets of carbide conglomerate projections are observed as shown in the insert in Fig. 7d. The needle-like projections belong to the carbide conglomerates with the plate plane parallel to the $(010)_\gamma$ crystallographic plane and the plate-like projections are from those with the plate plane parallel to the $(100)_\gamma$ crystallographic plane. The needle-like projection in Fig. 7d is composed of P-carbide sub-particles and the interspersed γ phase (γ_i) whose orientation has a 90° deviation from that of the surrounding γ matrix. While, the atomic arrangement differs among the P-carbides, the γ_i phase and the γ matrix are hardly discernible in the plate-like projection (Fig. 7e) as also found in our previous study [22]. This could be probably due to the small thickness of the carbide conglomerate, thus information comes from the carbide conglomerate and the γ matrix located above or below it. Viewing long the $[001]_\gamma$ orientation, cross-sections are observed to have regions of sub-carbide particles and the γ_i phase with an orientation 90° rotated with respect to the surrounding γ matrix. The carbide splitting phenomenon has also been found in the Ti-45Al-5Nb-(0.5-1)C alloys during annealing at 800 and 900 °C [20-22]. This suggests that the applied external stress shows no obvious influence on the morphology development of the P-carbides.

At a higher creep temperature of 850 °C under 260 MPa for 110 h, the interaction between the dislocations and P-carbides greatly increases, as shown in Fig. 8a. The dislocations are strongly pinned by the P-carbides densely nucleated along the dislocations and thus the creep resistance of the alloy should be improved by the precipitation strengthening mechanism [7, 15]. In addition, P-carbides in the γ phase are also observed to split (Fig. 8b). With further creep for 850 h, the P-carbides in the γ phase have disappeared and only a few P-carbides exist at dislocations and lamellar interfaces (Fig. 8c). Instead, more coarse P-carbides are found at grain boundaries. Compared to the situation at 750 °C, the P-carbides in the γ grain interior are less stable at 850 °C. Figs. 8d-e show the carbide precipitates in the specimens creep under 130 MPa for 1100 and 3267 h, respectively. After creep for 1100 h, only a few P-carbides are found at dislocations in the γ phase and at the lamellar interfaces. A redistribution of carbon from small carbides in the γ grain interior to large carbides at grain boundaries happens. Therefore, the carbon has mostly concentrated in the coarse carbides in sizes of tens to hundreds of nanometers after long-term creep [21, 29].

In SEM observation, elongated H-carbides are always found to form at the α_2 lath positions. This precipitation process should be induced by the dissolution of the α_2 laths during creep. Fig. 9 shows such H-carbides pictured by HRTEM. In Fig. 9a, a coarse H-carbide with long-periodic structure seems to nucleate at the α_2/γ interface and grows

at the expense of not only the α_2 lath but also the γ laths at both sides. These three phases follow the orientation relationships: $[101]_\gamma//[11\ \bar{2}\ 0]_H//[11\ \bar{2}\ 0]\alpha_2$ and $(11\bar{1})_\gamma//(0006)_H//(0002)\alpha_2$. The interface between the H-carbide and the α_2 phase is determined to be coherent while it is semi-coherent between the H-carbide and the γ phase as evidenced by the ledges at the interfaces. This can be explained by the lattice mismatch between these phases. According to the HEXRD results of this specimen, the lattice parameters are determined to be a=0.578 and c=0.466 nm for the α_2 phase, a=0.402 and c=0.408 nm for the γ phase, and a=0.305 and c=1.374 nm for the H phase. Then, the lattice mismatch is calculated to be $\frac{d_{(0002)\alpha2}-d_{(0006)H}}{d_{(0002)\alpha2}} = \frac{0.231-0.229}{0.231} = 0.9\%$ between the $(0002)_{\alpha2}$ and $(0006)_H$ planes and $\frac{d_{(11\bar{1})\gamma}-d_{(0006)H}}{d_{(11\bar{1})\gamma}} = \frac{0.233-0.229}{0.233} = 1.7\%$ between the $(11\bar{1})_\gamma$ and $(0006)_H$ planes. Thus, a smaller lattice mismatch exists between the H-carbide and the α_2 phase, and the small thickness of the α_2 lath also contributes to a coherent H-α_2 interface. It is also occasionally found that H-carbides precipitate within the γ laths with the above mentioned orientation relationship: $[101]_\gamma//[11\bar{2}0]_H$ and $(11\bar{1})_\gamma//(0006)_H$ as shown in Fig. 9b. It should be noted that the decomposition of α_2 lath proceeds with creep. Nano-sized fine α_2/γ lamellar structures are commonly found in long-term crept samples (Fig. 9c). As reported in literature [37, 38], the decomposition of α_2 laths is inevitable during long-term thermal exposure as well as in crept samples in different TiAl-based alloys, whereas in the present alloy this process is largely slowed down due to the stabilization of α_2 phase with carbon.

Combining the SEM, HEXRD and TEM results, the influences of the creep temperature, stress and time on the microstructure and carbide precipitation can be concluded as follows. With increasing the creep temperature and stress, the decomposition of the α_2 laths is more pronounced and the precipitation of H-carbides at the expense of the α_2 phase occurs at the γ/α_2 interfaces. With increasing creep time, the microstructure gets closer to thermodynamic equilibrium condition and the volume fraction of the α_2 phase is reduced accordingly. With respect to carbide precipitation, the volume fraction of carbides increases with creep temperature and time. While, the thermal stability of the P-carbides in the γ phase is reduced and redistribution of carbon from the small carbides in grain interior to the large carbides at grain boundaries occurs in a shorter creep time with increasing creep temperature. The creep stress plays no obvious role in the precipitation and morphology development of the P-carbides but influences greatly the formation of the H-carbides at γ/α_2 interfaces by affecting the stability of the α_2 laths in lamellar colonies.

3.4 Influence of carbon and microstructure on creep resistance

Based on the above results, the Ti-46Al-8Nb-0.7C alloy exhibits good creep resistance.

To the authors' knowledge, the creep property of this alloy is one of the best reported for polycrystalline TiAl alloys with nearly lamellar structure [39]. This can be attributed to the following factors. Firstly, high-Nb TiAl alloys are considered to have high strength because of the solid solution effect of Nb and C atoms, causing a higher critical stress to activate dislocations [40, 41]. Secondly, in the primary creep stage, the nearly fully lamellar microstructure has good thermal stability and the addition of carbon can further stabilize the α_2 phase and hinder the formation of β_o and ω_o phases [18]. As creep cavities tend to form along the grain boundaries of equiaxed γ grains rather than within the lamellar colonies [35, 36], the good microstructural stability can contribute to the good creep resistance by reducing the formation of equiaxed γ grains. Thirdly, the precipitation of the P-carbides at dislocations in the γ phase can pin the dislocations and strongly slow down and hinder their glide. The closely distributed P-carbides at the lamellar interfaces could also play a role in preventing the activation of bow-out interface dislocations under stress [39]. Compared to smaller and densely dispersed P-carbides, H-type carbides in the γ phase might be less beneficial for improving creep properties. However, for the H-carbides distributing along the γ/α_2 interfaces, a number of studies reported that they were beneficial for creep resistance because the elongated H-carbides acted as hard-phase islands to preserve the γ/α_2 interfaces and restrict the movement of interfacial dislocations [32-34]. Recent investigations also reported that the random primary H-carbides could enhance the fracture toughness and creep resistance of carbon containing high Nb-TiAl alloys by restraining the crack propagation [24, 42]. Thus, the precipitation of H-carbides at the γ/α_2 interfaces is supposed to contribute to a better creep resistance of the Ti-46Al-8Nb-0.7C alloy. As the creep proceeds, more and more fine P-carbides precipitate in the γ phase. However, there should be a certain moment when the supersaturation of the γ phase with C is exhausted by carbide precipitation. Then the coarsening of carbides and redistribution of carbon to large grain boundary carbides have become the main trends of microstructure evolution. As a result, the pinning effect on dislocations starts to decrease. This can be a very long period since even in the samples after 1100 h creep the carbides can still be observed in γ grain interior. In the third stage of creep, the coarse carbides may have limited effect on the pinning of dislocations. Therefore, the dislocations would have more free space to glide without obstacles. Moreover, the decomposition of α_2 phase introduces numerous new lamellar interfaces, which further provide extra dislocation sources and more volume of deformable γ phase free of carbides. However, it should be noted that the overall ductilities of the creep samples are all very low (less than 3%), meaning that the dislocation movement cannot be comprehensively activated in the whole sample. The recrystallized γ grains at the lamellar colony boundaries could contribute to the overall deformation. But this can only be effective after long-term annealing. Additionally, the newly formed γ grains at

lamellar colony boundaries would also contribute to grain boundary gliding. This can explain the sudden increase of the strain rate in the last section of the creep curve. The difference in the creep life of the samples deformed at 750 and 850 ºC possibly comes from the dislocation climb mechanism, which is less active at lower temperatures.

4. Conclusions

In this study, the creep properties and the effects of creep temperature, stress and time on the microstructural evolution and carbide precipitation in a high Nb-TiAl alloy are investigated during creep at intermediate temperatures. The main results are concluded as follows.

(1) The Ti-46Al-8Nb-0.7C alloy exhibits good creep resistance and the creep life is 850 h and 3267 h for samples crept at 850 ℃/260 MPa and 850 ℃/130 MPa, respectively. The creep life of the sample crept at 750 ℃ and 260 MPa is more than 8500 h without rupture.

(2) The Ti-46Al-8Nb-0.7C alloy shows good microstructural stability during creep at intermediate temperatures. The microstructure is slightly decomposed by formation of equiaxed γ grains at the lamellar boundaries and the decomposition of α_2 laths which is more obvious at higher creep temperature and stress.

(3) Numerous P-carbides precipitate in the γ laths and equiaxed γ grains, which can hinder the dislocation motion and thus improve the creep resistance. The decomposition of the α_2 laths induced H-carbide precipitation at the γ/α_2 lamellar interfaces. The interfacial H-carbides can preserve the γ/α_2 interfaces and restrict the movement of interfacial dislocations, and thus improve the creep resistance.

(4) The volume fraction of carbides increases with creep temperature and time. However, the creep stress hardly affects the precipitation and morphology development of the P-carbides but a higher stress can promote the precipitation of H-carbides at γ/α_2 interfaces by destabilizing the α_2 laths in the lamellar colonies.

Acknowledgments

This work was supported by the National Natural Science Foundation of China (contract No. 51601146), State Key Lab of Advanced Metals and Materials (contract No. 2017-ZD02), and Natural Science Basic Research Plan of Shaanxi Province (contract No. 2017JQ5006). Li Wang acknowledges the financial support from the Helmholtz Association in the frame of Helmholtz Postdoc Program. Lin Song acknowledges the fruitful discussion with Dr. J.D.H. Paul and his help on the creep tests.

References

[1] Y.W. Kim, S.L. Kim, Advances in Gammalloy Materials-Processes-Application Technology: Successes, Dilemmas, and Future, JOM (2018).

[2] H. Clemens, S. Mayer, Design, Processing, Microstructure, Properties, and Applications of Advanced Intermetallic TiAl Alloys, Adv. Eng. Mater. 15 (2013) 191-215.
[3] H. Clemens, H. Kestler, Processing and Applications of Intermetallic γ-TiAl-Based Alloys, Adv. Eng. Mater. 2 (2000) 551-570.
[4] F. Appel, U. Brossmann, U. Christoph, S. Eggert, P. Janschek, U. Lorenz, J. Müllauer, M. Oehring, J.D.H. Paul, Recent Progress in the Development of Gamma Titanium Aluminide Alloys, Adv. Eng. Mater. 2 (2000) 699-720.
[5] R. Chen, Q. Wang, Y. Yang, J. Guo, Y. Su, H. Ding, H. Fu, Brittle–ductile transition during creep in nearly and fully lamellar high-Nb TiAl alloys, Intermetallics 93 (2018) 47-54.
[6] M. Kastenhuber, B. Rashkova, H. Clemens, S. Mayer, Enhancement of creep properties and microstructural stability of intermetallic β-solidifying γ-TiAl based alloys, Intermetallics 63 (2015) 19-26.
[7] Y.W. Kim, S.L. Kim, Effects of microstructure and C and Si additions on elevated temperature creep and fatigue of gamma TiAl alloys, Intermetallics 53 (2014) 92-101.
[8] T. Klein, L. Usategui, B. Rashkova, M.L. Nó, J.S. Juan, H. Clemens, S. Mayer, Mechanical behavior and related microstructural aspects of a nano-lamellar TiAl alloy at elevated temperatures, Acta Mater. 128 (2017) 440-450.
[9] W. Qi, R. Chen, G. Xue, J. Guo, Y. Su, H. Ding, H. Fu, Microstructure control and creep behavior of Ti-47Al-6Nb-0.1C alloy by directional solidification, Intermetallics 94 (2018) 152-159.
[10] H. Zhu, D.Y. Seo, K. Maruyama, P. Au, Effect of microstructural stability on creep behavior of 47XD TiAl alloys with fine-grained fully lamellar structure, Scripta Mater. 52 (2005) 45-50.
[11] M. Kastenhuber, B. Rashkova, H. Clemens, S. Mayer, Effect of microstructural instability on the creep resistance of an advanced intermetallic γ-TiAl based alloy, Intermetallics 80 (2017) 1-9.
[12] S. Karthikeyan, M.J. Mills, The role of microstructural stability on compression creep of fully lamellar γ-TiAl alloys, Intermetallics 13 (2005) 985-992.
[13] H. Zhu, D.Y. Seo, K. Maruyama, Effect of lamellar spacing on microstructural instability and creep behavior of a lamellar TiAl alloy, Scripta Mater. 54 (2006) 1979-1984.
[14] W.H. Tian, M. Nemoto, Effect of carbon addition on the microstructures and mechanical properties of γ-TiAl alloys, Intermetallics 5 (1997) 237-244.
[15] E. Schwaighofer, B. Rashkova, H. Clemens, A. Stark, S. Mayer, Effect of carbon addition on solidification behavior, phase evolution and creep properties of an intermetallic β-stabilized γ-TiAl based alloy, Intermetallics 46 (2014) 173-184.
[16] F. Appel, U. Christoph, R. Wagner, Solution and Precipitation Hardening in Carbon-Doped Two-Phase γ-Titanium Aluminides, Mrs Proceedings 460 (1996) 77.
[17] U. Christoph, F. Appel, R. Wagner, Dislocation dynamics in carbon-doped titanium aluminide alloys, Mater. Sci. Eng. A 239-240 (1997) 39-45.
[18] T. Klein, M. Schachermayer, F. Mendez-Martin, T. Schöberl, B. Rashkova, H. Clemens, S. Mayer, Carbon distribution in multi-phase γ -TiAl based alloys and its influence on mechanical properties and phase formation, Acta Mater. 94 (2015) 205-213.
[19] H.S. Park, S.W. Nam, N.J. Kim, S.K. Hwang, Refinement of the lamellar structure in TiAl-based intermetallic compound by addition of carbon, Scripta Mater. 41 (1999) 1197-1203.

[20] J. Lapin, T. Pelachová, O. Bajana, High temperature deformation behaviour and microstructure of cast in-situ TiAl matrix composite reinforced with carbide particles, J. Alloy. Compd. 797 (2019) 754-765.
[21] L. Wang, U. Lorenz, M. Münch, A. Stark, F. Pyczak, Influence of alloy composition and thermal history on carbide precipitation in γ-based TiAl alloys, Intermetallics 89 (2017) 32-39.
[22] L. Wang, M. Oehring, U. Lorenz, A. Stark, F. Pyczak, New insights into perovskite-Ti_3AlC precipitate splitting in a Ti-45Al-5Nb-0.75C alloy by transmission electron microscopy, Intermetallics 100 (2018) 70-76.
[23] L. Wang, C. Zenk, A. Stark, P. Felfer, H. Gabrisch, M. Göken, U. Lorenz, F. Pyczak, Morphology evolution of Ti_3AlC carbide precipitates in high Nb containing TiAl alloys, Acta Mater. 137 (2017) 36-44.
[24] J. Lapin, K. Kamyshnykova, Processing, microstructure and mechanical properties of in-situ Ti_3Al+TiAl matrix composite reinforced with Ti_2AlC particles prepared by centrifugal casting, Intermetallics 98 (2018) 34-44.
[25] X. Hu, J. Li, L. Song, T. Zhang, Coupling effects of deformation and thermal exposure on the precipitation behaviors of βo(ω) phases in a high Nb-containing TiAl alloy, Mater. Des. 148 (2018) 135-144.
[26] L. Song, L.Q. Zhang, X.J. Xu, J. Sun, J.P. Lin, Omega phase in as-cast high-Nb-containing TiAl alloy, Scripta Mater. 68 (2013) 929-932.
[27] Z.W. Huang, Thermal stability of Ti–44Al–4Nb–4Zr–0.2Si–1B alloy, Intermetallics 42 (2013) 170-179.
[28] Z.W. Huang, D.G. Zhu, Thermal stability of Ti–44Al–8Nb–1B alloy, Intermetallics 16 (2008) 156-167.
[29] L. Wang, H. Gabrisch, U. Lorenz, F.P. Schimansky, A. Schreyer, A. Stark, F. Pyczak, Nucleation and thermal stability of carbide precipitates in high Nb containing TiAl alloys, Intermetallics 66 (2015) 111-119.
[30] H. Gabrisch, A. Stark, F.P. Schimansky, L. Wang, N. Schell, U. Lorenz, F. Pyczak, Investigation of carbides in Ti-45Al-5Nb-xC alloys ($0 \leq x \leq 1$) by transmission electron microscopy and high energy-XRD, Intermetallics 33 (2013) 44-53.
[31] T. Ye, L. Song, S. Gao, Y. Liang, Y. Wang, J. Lin, Precipitation behavior of the ω_o phase in an annealed high Nb-TiAl alloy, J. Alloy. Compd. 701 (2017) 882-891.
[32] P.I. Gouma, K. Subramanian, Y. W. Kim, M. J. Mills, Annealing studies of γ-titanium aluminides alloyed with light elements for creep strengthening, Intermetallics 6 (1998) 689-693.
[33] P.I. Gouma, M. J. Mills, Characterization of the precipitation process in a TiAl-based alloy with carbon and silicon additions, Philos. Mag. Lett. 78 (1998) 59-66.
[34] M. Karadge, P. I. Gouma, Y. W. Kim, Precipitation strengthening in K5-series γ-TiAl alloyed with silicon and carbon, Metall. Mater. Trans. A 34 (2003) 2129-2138.
[35] X.W. Du, J. Zhu, Y.W. Kim, Microstructural characterization of creep cavitation in a fully-lamellar TiAl alloy, Intermetallics 9 (2001) 0-146.
[36] M.E. Kassner, T.A. Hayes, Creep cavitation in metals, Int. J. Plasticity 19 (2003) 1715-1748.
[37] Z.W. Huang, T. Cong, Microstructural instability and embrittlement behaviour of an Al-lean, high-Nb γ-TiAl-based alloy subjected to a long-term thermal exposure in air,

Intermetallics 18 (2010) 161-172.
[38] S. Bystrzanowski, A. Bartels, H. Clemens, R. Gerling, F.P. Schimansky, G. Dehm, H. Kestler, Creep behaviour and related high temperature microstructural stability of Ti–46Al–9Nb sheet material, Intermetallics 13 (2005) 515-524.
[39] F. Appel, J.D.H. Paul, M. Oehring, Creep, in: Gamma Titanium Aluminide Alloys, Wiley-VCH Verlag GmbH & Co. KGaA, 2011 pp. 313-356.
[40] F. Appel, M. Oehring, R. Wagner, Novel design concepts for gamma-base titanium aluminide alloys, Intermetallics 8 (2000) 1283-1312.
[41] G.E. Bean, M.S. Kesler, M.V. Manuel, Effect of Nb on phase transformations and microstructure in high Nb titanium aluminides, J. Alloy. Compd. 613 (2014) 351-356.
[42] J. Lapin, A. Klimová, Z. Gabalcová, T. Pelachová, O. Bajana, M. Štamborská, Microstructure and mechanical properties of cast in-situ TiAl matrix composites reinforced with $(Ti,Nb)_2AlC$ particles, Mater. Des. 133 (2017) 404-415.

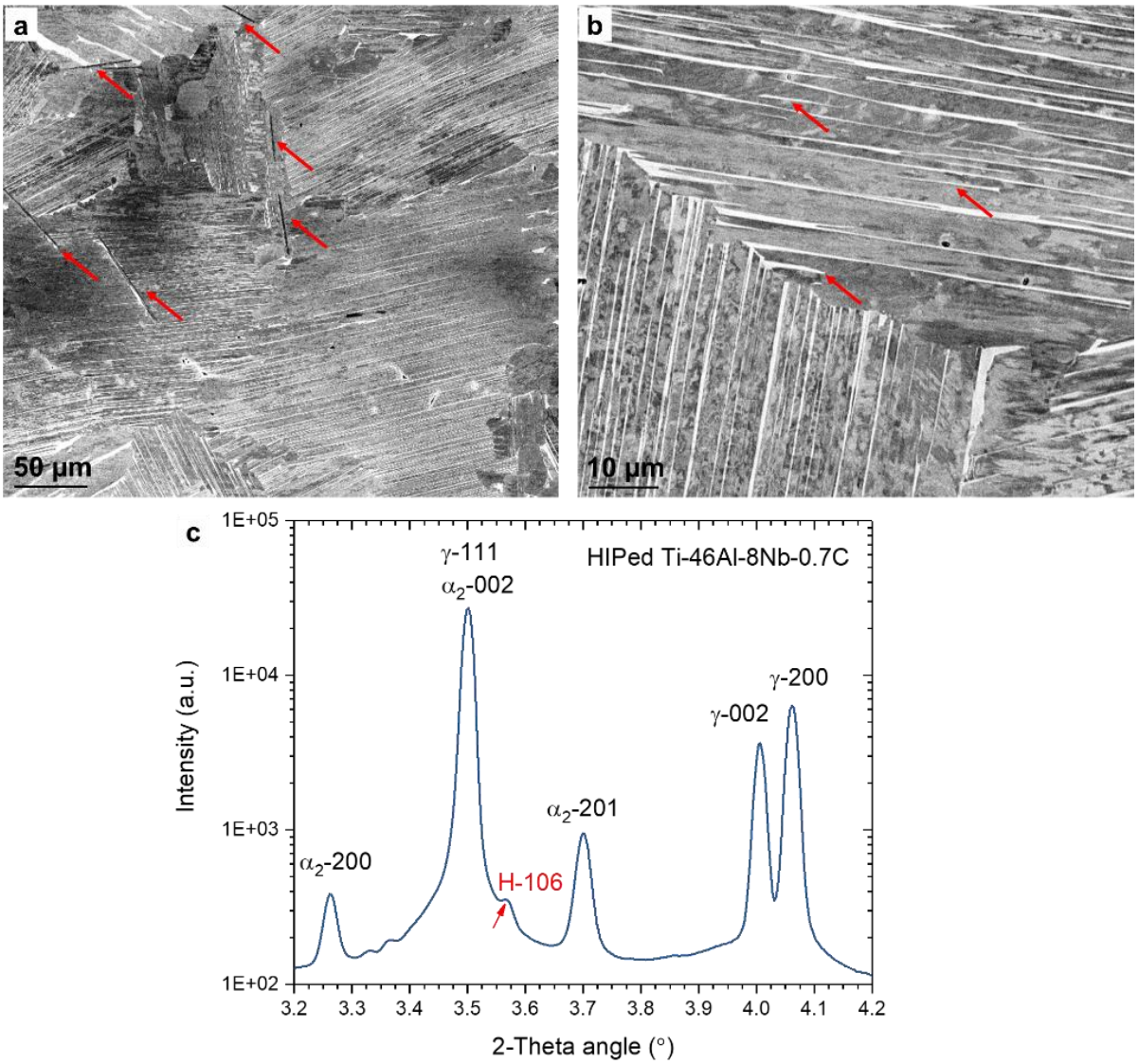

Fig. 1 Microstructure and phase constitution of the as-HIPed sample. (a, b) SEM images in back-scattered electron mode (the arrows in (a) and (b) indicate the locations of the H-carbides and the fractured α_2 laths, respectively); (c) HEXRD spectrum, the {106} peak of H-carbides is observed

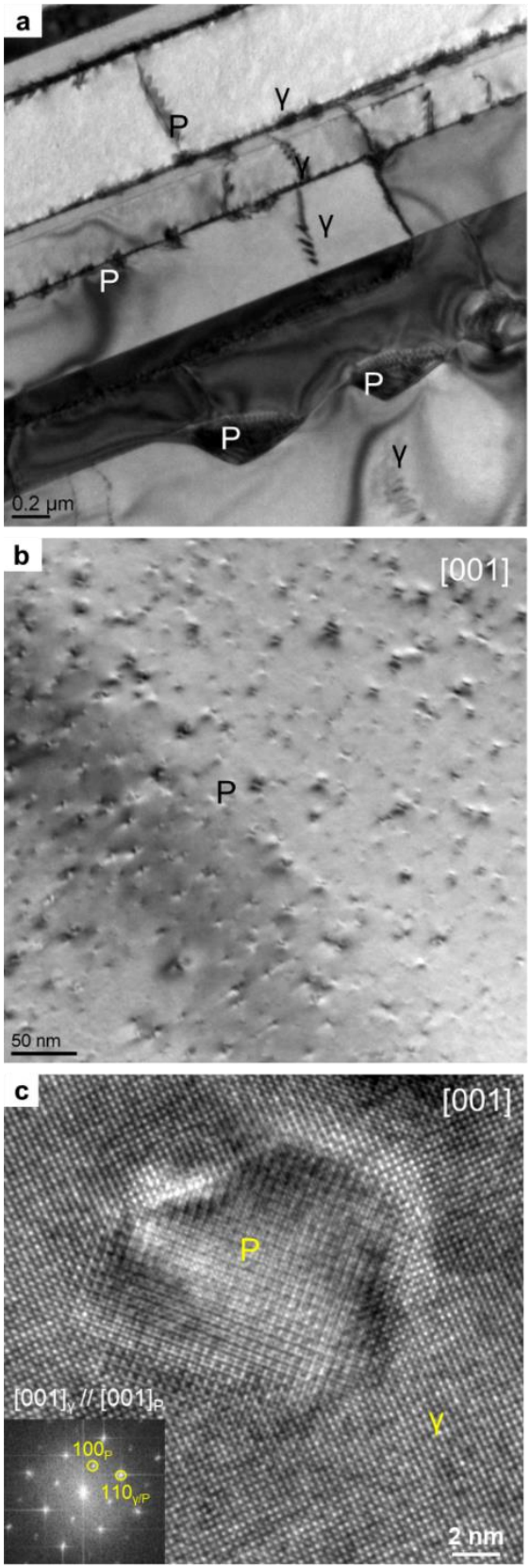

Fig. 2 TEM investigations on the distribution of P-carbides in the as-HIPed sample. (a) P-carbides exist at boundaries, γ twin interfaces and at dislocations, (b) in the γ matrix and (c) P-phase at atomic resolution imaged along the $[001]_\gamma$ zone axis

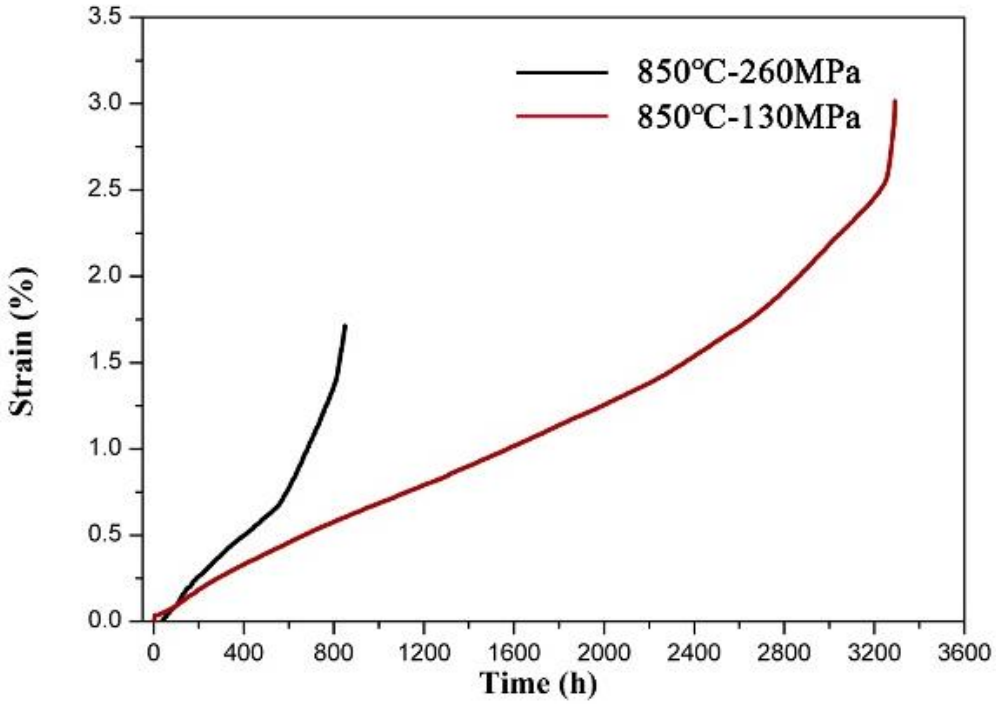

Fig. 3 Creep curves of the samples tested at 850 °C under tensile stresses of 130 and 260 MPa

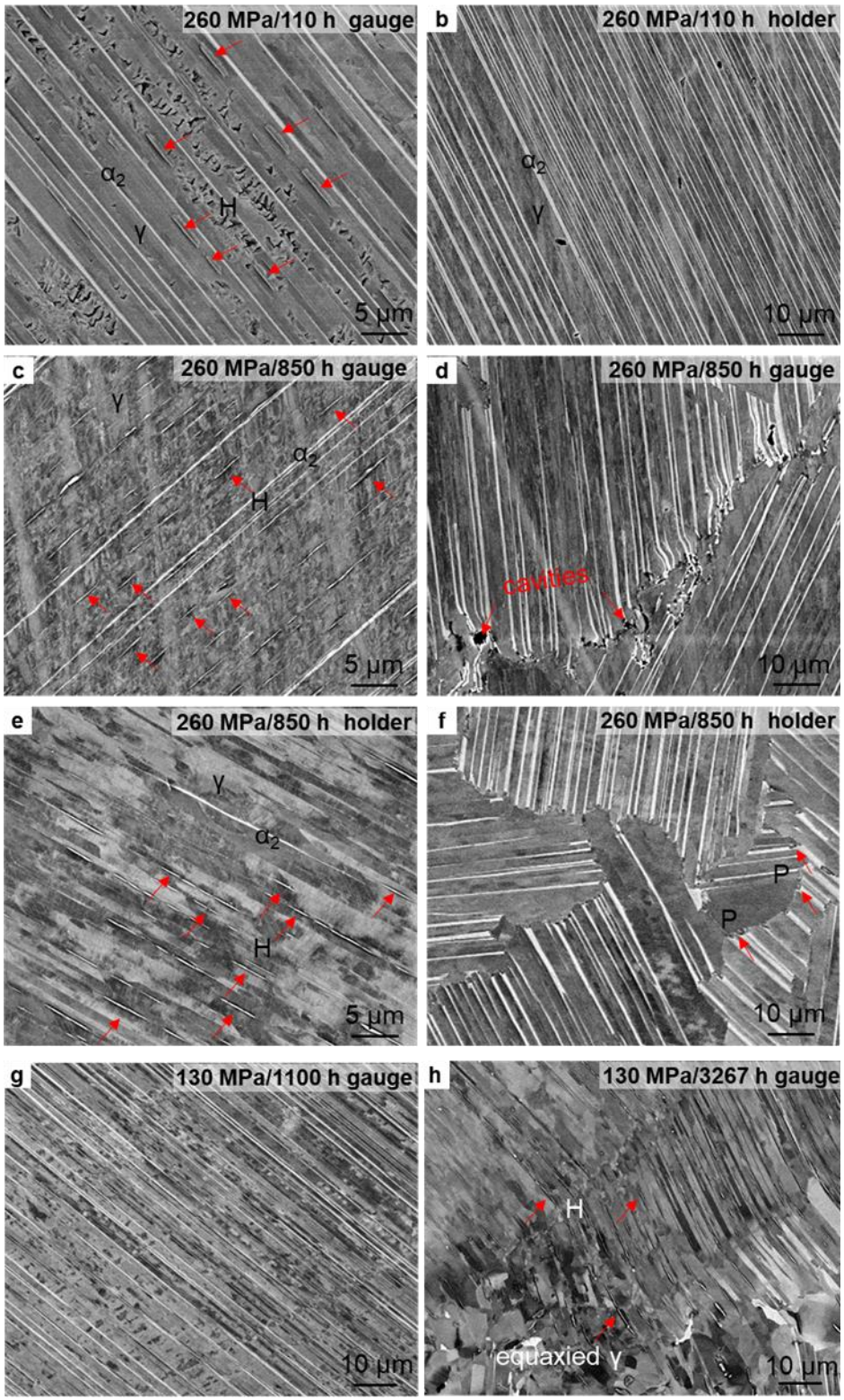

Fig. 4 SEM investigations in back-scattered electron mode of the microstructure evolution during creep at 850 °C for different times. (a) 260 MPa/110 h, in the gauge section, (b) 260 MPa/110 h, in the holder section, (c, d) 260 MPa/850 h, in the gauge section, and (e, f) 260 MPa/850 h, in the holder section, (g) 130 MPa/1100 h, in the gauge section, (h) 130 MPa/3267 h, in the gauge section

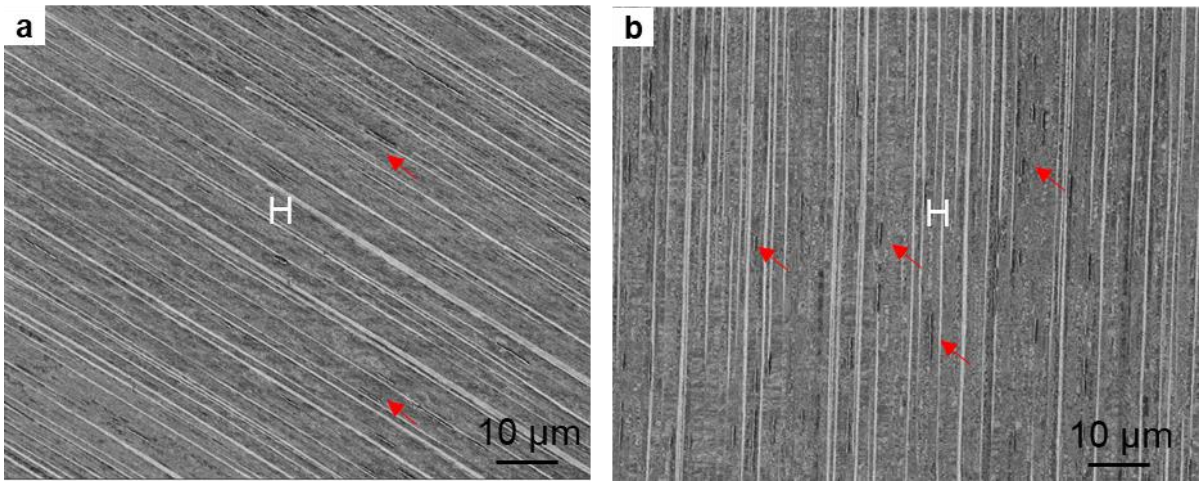

Fig. 5 SEM investigations in back-scattered electron mode of the microstructure evolution during creep at 750 °C for 1200 h in the gauge section under stress of (a) 130 and (b) 260 MPa

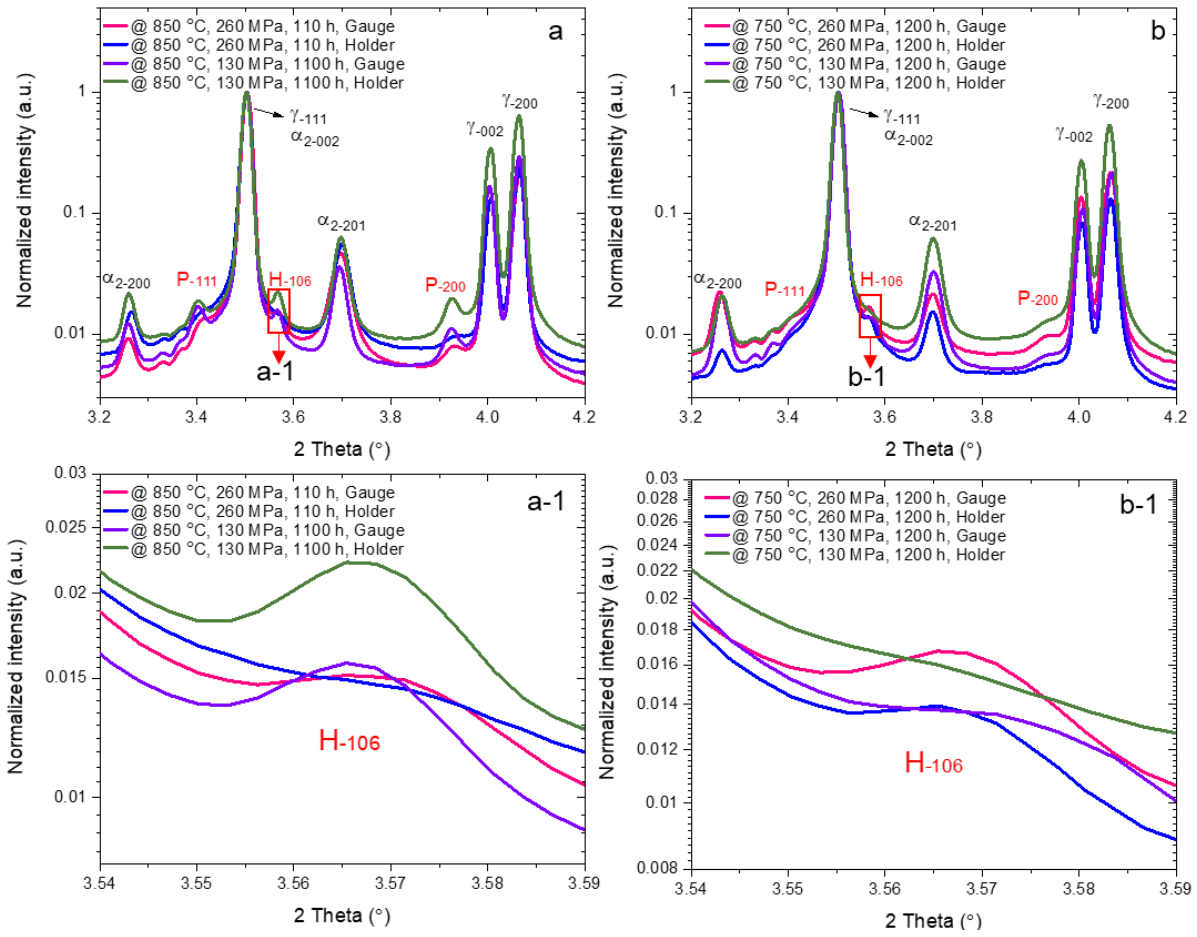

Fig. 6 HEXRD spectrums of specimens after creep. (a) Crept at 850 ℃, (a-1) enlarged spectrums for the marked region in (a), (b) crept at 750 ℃, and (b-1) enlarged spectrums for the marked region in (b)

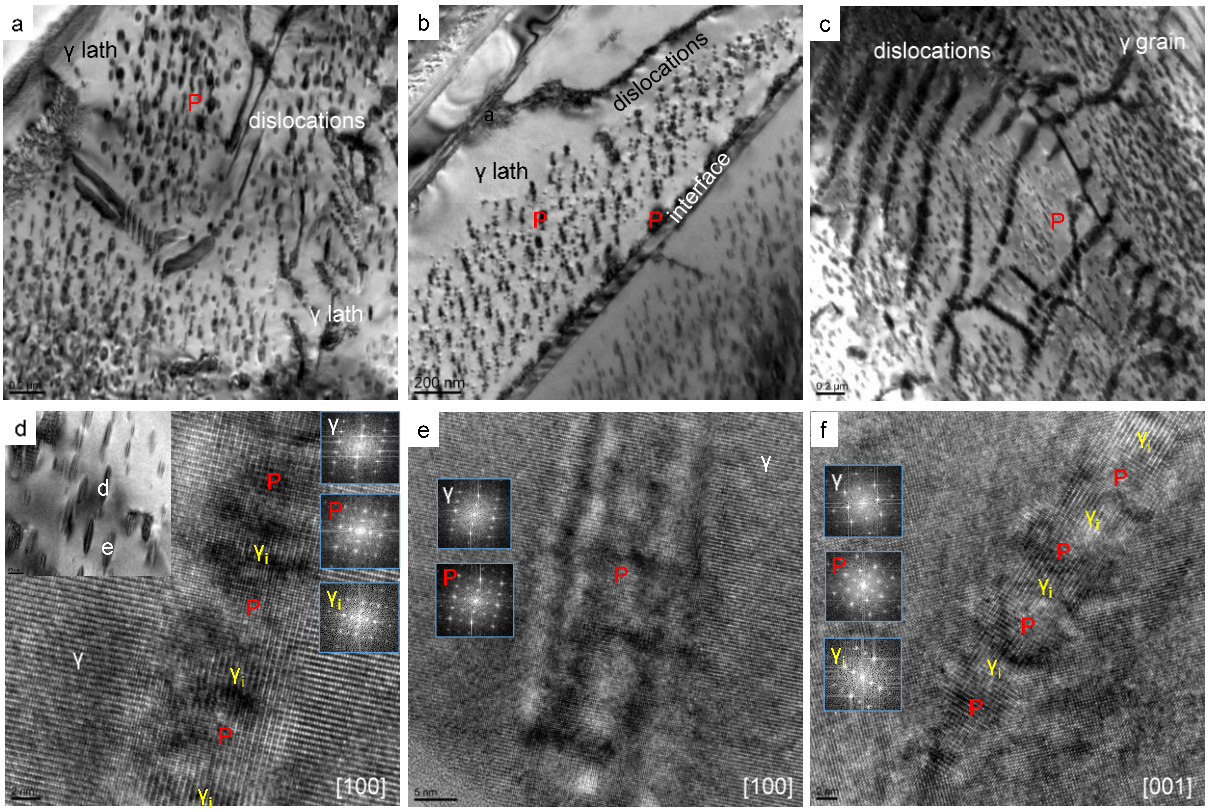

Fig. 7 TEM and HRTEM investigation of the P-carbides in specimens crept at 750 °C for 1200 h. P-carbides form (a) in the γ laths, (b) along the lamellar interfaces and (c) in the γ grains. P-carbides split in the γ phase (d, e, and f). (d) The needle-like projection of a carbide conglomerate viewed along the $[100]_\gamma$ orientation, the inserted image is a low magnification of d and e, (e) the plate-like projection of a carbide conglomerate recorded along the $[100]_\gamma$ orientation, and (f) the cross-section of a carbide conglomerate along the $[001]_\gamma$ orientation

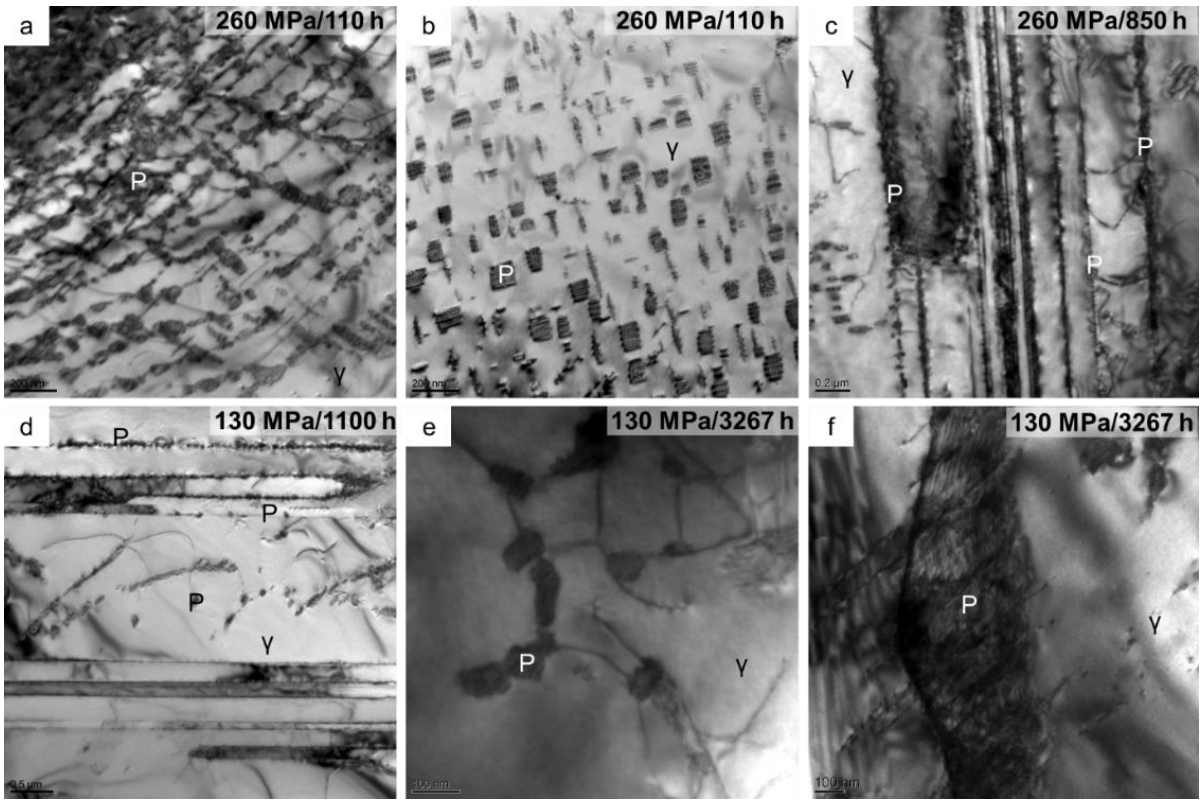

Fig. 8 TEM of the P-carbides in the specimens crept at 850 °C for different times: under 260 MPa for 110 h (a) P-carbides interact with dislocations, (b) P-carbides split in the γ phase; under 260 MPa for 850 h (c) P-carbides at dislocations and lamellar interfaces; under 130 MPa for 1100 h (d) P-carbides at dislocations and lamellar interfaces; under 130 MPa for 3267 h (e) only a few P-carbides remain at dislocations and lamellar interfaces, and (f) coarse P-carbides exist at grain boundaries

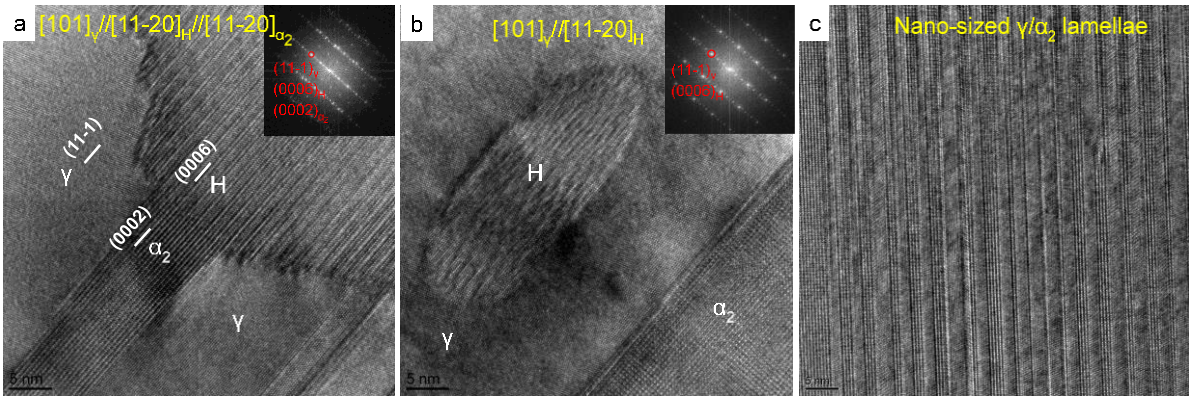

Fig. 9 HRTEM investigation of the H-carbides. (a) H-carbides form along the γ/α_2 interfaces (b) H-carbides precipitate in the γ lath, and (c) α_2 laths have decomposed into nano-sized γ/α_2 lamellae

Table 1 The creep test results in the Ti-46Al-8Nb-0.7C alloy

Temperature	stress	Time	strain	state
850 ℃	260 MPa	850 h	1.7 %	rupture
850 ℃	130 MPa	3267 h	3.0 %	rupture
750 ℃	260 MPa	> 8500 h	> 1.3 %	unfaulted
750 ℃	130 MPa	> 1200 h	> 0.2 %	unfaulted

Table 2 The creep properties of TiAl alloys with varied compositions reported in the literature

Composition (at.%)	Microstructure	Parameters	Creep time	Creep strain	Refs
Ti-45Al-8.5Nb-0.2W-0.2B-0.02Y	Duplex	850 °C, 130 MPa	68 h	27%	[3]
Ti-44Al-8Nb-0.2W-0.2B-0.1Y	NFL	800 °C, 200 MPa	147 h	6.0 %	[4]
Ti-44Al-6Nb-1Cr-2V	NFL	800 °C, 150 MPa	~600 h	~20 %	[5]
Ti-43.5Al-4Nb-1Mo-0.1B	NFL	815 °C, 150 MPa	~120 h	~6.2 %	[6]
Ti-43Al-4Nb-1Mo-0.1B-0.3C-0.3Si	NFL	815 °C, 150 MPa	~210 h	~3.0 %	[6]
Ti-46Al-3Nb-2Cr-0.2W	FL	760 °C, 276 MPa	138 h	1.4 %	[7]
Ti-46Al-3Nb-2Cr-0.2W-0.2Si-0.2C	FL	760 °C, 276 MPa	125 h	1.3 %	[7]
Ti-44Al-6Nb-1Cr-2V	NFL	800 °C, 276 MPa	~50 h	~21%	[8]
Ti-47Al-6Nb-0.1C	FL	800 °C, 276 MPa	~160 h	~5.0 %	[8]
Ti-47Al-6Nb-0.1C	FL	800 °C, 200 MPa	850 h	~6.0 %	[9]

Table 3 The α_2 phase fraction in the holder section of the crept samples after testing at different conditions. The α_2 phase fraction in the HIPed sample is also shown for comparison

Creep conditions	α_2 phase fraction, wt.%
HIPed state	12.9
@ 750 ℃, 130 MPa, 1200 h	9.2
@ 850 ℃, 130 MPa, 1100 h	8.0
@ 850 ℃, 130 MPa, 3267 h	6.5
@ 850 ℃, 260 MPa, 110 h	8.3
@ 850 ℃, 260 MPa, 850 h	4.5